

Gas and dust in the Ophiuchus region

J. de Geus^{1,2} and W.B. Burton¹

Sterrewacht Leiden, Postbus 9513, NL-2300 RA Leiden, The Netherlands
Astronomy Program, University of Maryland, College Park, MD 20742, USA

Received May 23, accepted August 30, 1990

Abstract. The interstellar gas and dust in the Ophiuchus molecular cloud region are studied through HI, CO and IRAS observations. The generally good global correlation of HI with the infrared intensity and dust optical depth breaks down on the smaller scales that can be distinguished in this nearby region. The presence of an intense ultraviolet field and shocks caused by the early-type stars account for this difference. Integrated emission from the CO molecule correlates with the dust optical depth. This correlation is used to derive the conversion factor between W_{CO} and the atomic hydrogen column density. The region close to the early-type stars in Upper Scorpius shows a considerable amount of infrared emission, but negligible CO emission. The infrared structures in the latter region generally have HI counterparts. The HI is most likely the dissociated remnant of the molecular cloud. From a comparison of the visual extinction towards the stars with the infrared intensities in the same directions, the distance to the far edge of the Ophiuchus clouds is derived at 200 pc.

Key words: interstellar medium: clouds: Ophiuchus – interstellar medium: dust – interstellar medium: molecules

1. Introduction

Knowledge of the distribution of an important constituent of the interstellar medium, dust, was greatly improved by the results of the IRAS mission. Large scale studies have benefitted from the mapping abilities of the satellite. Such studies have involved comparison of different tracers of the interstellar gas with emission from dust, not only on the large scales appropriate to the study of the global morphology of the Galaxy (Sodroski et al. 1987; Burton & Deul 1988; Boulanger & Perault 1988), but also on the smaller scales characteristic of cirrus structures (Boulanger et al. 1985; Tereby & Fich 1986; Schwering 1988). These previous studies have concentrated on comparison of emission from dust with that from atomic hydrogen gas. It was found that these two components are generally well correlated, although the details of the correlations vary from one region to another. The differences are usually ascribed to variations in the physical properties of the dust particles, such as size distribution and temperature, both of which are influenced by the strength of the interstellar radiation field (ISRF) and by the occurrence of shocks (Draine & Lee 1984). It is natural to consider the correlations between HI and dust in a

starforming region, where a large number of early-type stars is present, so that the ISRF is enhanced, and shocks are abundant.

The Ophiuchus clouds, at a distance of only about 125 pc, are well suited for such a study. The clouds are believed to be the remnant of a giant molecular cloud from which the stars of the Scorpio-Centaurus OB association were formed (see Blaauw 1964). The youngest subgroup of the association, Upper Scorpius, contains several stars which show interaction with gas in the Ophiuchus region. On the largest scales the interstellar matter of the Ophiuchus/Upper-Scorpius region is characterized by the presence of neutral hydrogen up to $+40^\circ$ out of the plane (see e.g. Colomb et al. 1980). The high-latitude clouds detected by Magnani et al. (1985) in this region at $b > 35^\circ$ are likely to be associated with the clouds in the Ophiuchus region. At specific velocities ($v \sim +5 \text{ km s}^{-1}$) the atomic hydrogen shows a loop-like structure surrounding the early-type stars in Upper Scorpius (Cappa de Nicolau & Pöppel 1986). The Ophiuchus molecular clouds generally reside inside the perimeter of this loop. Several atomic hydrogen structures are positioned close to the molecular clouds, and are likely to be physically related to them. The molecular clouds are generally elongated (Vrba 1977; Vrba et al. 1975; de Geus et al. 1990 hereafter Paper II), with directions that do not appear to be random. Comparison of the shape of the clouds with the distribution of other tracers in the region may shed some light on the origin of the structures.

Cappa de Nicolau & Pöppel (1986, hereafter CdNP) made an extensive kinematical study of the atomic hydrogen component in the region of Ophiuchus/Upper Scorpius. They compared the neutral hydrogen distribution with available tracers of the molecular gas, with studies of the ionized component, and with absorption-line observations. They found a weak correlation between the visual extinction (based on star counts) and the neutral hydrogen column density. No comparison, however, could be made between the large scale distributions of the dense gas and dust and the neutral hydrogen. The availability of the CO survey (Paper II) and the IRAS maps now enables us to make a full comparison of the distributions of these components in the entire region.

Ionized gas is an important component of the interstellar medium, especially in the vicinity of early-type stars. Several stars in Upper Scorpius indeed have H II regions around them, such as S1 (Sharpless 1959) around π Sco, S7 around δ Sco, S9 around σ Sco, S27 around ζ Oph, and RCW 129 (Rodgers et al. 1960) around τ Sco. Furthermore, the 2.3-GHz radio-continuum survey by Baart et al. 1980 revealed the presence of a considerable amount of diffuse ionized gas associated with the general region of Upper Scorpius. The relation between the ionized and atomic gas

Send offprint requests to: E.J. de Geus (Maryland address)

was shown by CdNP to be rather complex. The H II regions around π and δ Sco were found to be associated with a hole in the distribution of H I, whereas the ionized gas around σ Sco is associated with an H I cloud.

In this paper, the global correlation between gas and dust is investigated on a range of scales within the Ophiuchus region, using the IRAS data, the Leiden-Green Bank H I survey (Burton 1985) together with new higher-resolution H I observations, and the ^{12}CO survey of the Ophiuchus region (Paper II). An independent tracer of the dust is given by the visual extinctions towards the stars in the Upper-Scorpius region. The extinctions were calculated by de Geus et al. (1989 hereafter Paper I) and are compared here with the infrared intensities measured by IRAS at 60 and 100 μm . This provides information on the location of the stars, and allows a derivation of the extent of the Ophiuchus cloud along the line of sight.

2. Data presentation

2.1. The IRAS maps

The IRAS mission, instruments, and calibration procedures are described in the IRAS Explanatory Supplement (1985). The IRAS product currently best suited for a study of the correlation of the infrared emission with the atomic and molecular gas over large areas of sky is the collection of Skyflux maps. At all four IRAS wavelengths, three different sets of Skyflux maps are available (HCON's 1, 2, and 3), each observed at a different epoch. In the region of Ophiuchus each HCON unfortunately misses a number of lunes (scans of the IRAS telescope in ecliptic latitude at constant longitude). In order to get a more complete map of the dust distribution in this part of the sky, HCON's 1 and 2 were combined. This combined map still contained a gap of about $6^\circ \times 0^\circ.6$ extent, located near the center of the ρ Oph cloud. This remaining gap was filled in with data from HCON 3. Because contamination by zodiacal dust is much larger in HCON 3 than in HCON's 1 and 2, HCON 3 was used only in this small area. This reduces calibration problems when subtracting the zodiacal emission from the maps. Complete maps at all four IRAS wavelengths were constructed of the area enclosed by $l = 355^\circ \pm 30^\circ$ and $b = 15^\circ \pm 30^\circ$, with a resolution of $0^\circ.06$.

2.1.1. Correction for zodiacal contamination

It is an unfortunate circumstance that the region of the Ophiuchus molecular clouds has an ecliptic latitude $\beta \sim 0^\circ$. All four IRAS bands are therefore strongly influenced by emission from zodiacal dust. Several methods have been deployed in recent studies for determining the zodiacal contribution in the four IRAS bands. We have combined aspects of two papers (Deul & Wolstencroft 1988; Walterbos & Schwering 1987) to derive a correction for the zodiacal dust emission, appropriate for the Ophiuchus region.

Following Walterbos & Schwering (1987), we spectrally decomposed the emission in the four wavelength bands into the contributions from three components characterized by different dust temperatures. The zodiacal component was assumed to be at 200 K. An important condition that must be met is, that the Galactic object under study does not contain dust at temperatures similar to that of the zodiacal dust. In the case of the Ophiuchus region small scale structure was indeed found in the "hot dust" decomposition, associated with the hot stars in the region. However, due to the difference in angular scale between the

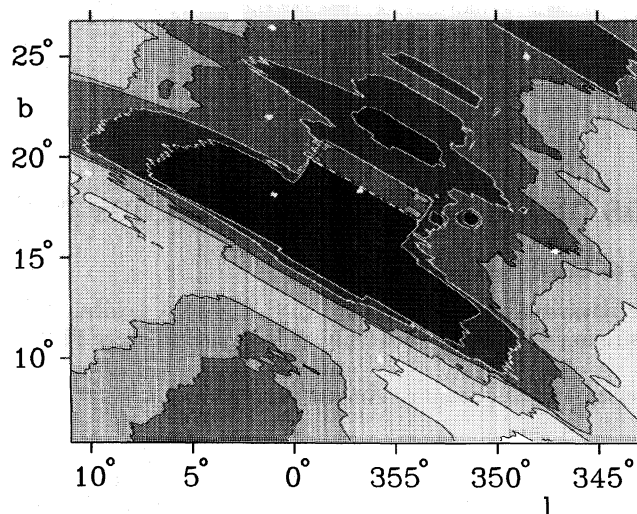


Fig. 1. Map in Galactic coordinates of the zodiacal emissivity for the region of the Ophiuchus molecular clouds. Note that zero ecliptic latitude unfortunately passes through the Ophiuchus region. The units of the map are arbitrary

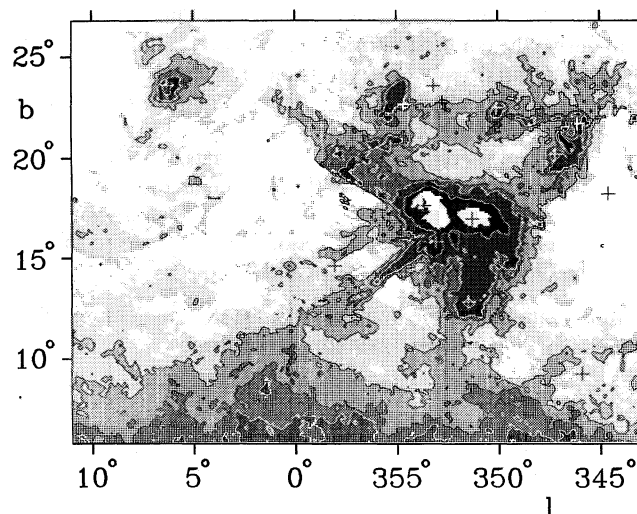


Fig. 2. Map of 60- μm intensities corrected for zodiacal emissivity, showing the distribution of interstellar dust in the Ophiuchus region. The contour values are 8, 11.5, 15, and 30 MJy/sr

zodiacal and Ophiuchus contributions, the latter could be filtered out using a 9-point median filter (applied in the ecliptic-latitude direction). The resulting map of the zodiacal emissivity in the Ophiuchus region is shown in Fig. 1. The intensities of this map were then scaled to the model of Deul & Wolstencroft (1988) to fit the intensities of the zodiacal contribution in all four bands. Figures 2 and 3 show the distribution of dust emission at 60 and 100 μm in the Ophiuchus region after subtraction of the zodiacal contamination.

2.1.2. Dust temperature and optical depth

The infrared intensity measured in each of the four IRAS wavelength bands represents emission by dust particles of different sizes, temperatures, and column densities. The intensity at frequency ν is given by $I_\nu = B_\nu(T) \cdot \tau_\nu$, with $B_\nu(T)$ the Planck

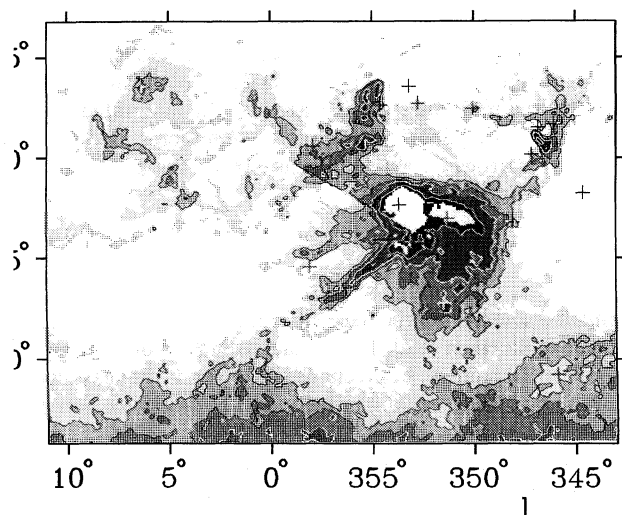


Fig. 3. Map of 100- μm intensities corrected for zodiacal emissivity. The Ophiuchus dust complex shows a variety of cloud structures, some of which are highly elongated. The contour values are 40, 55, 75 and 135 MJy/sr

extinction intensity at that frequency and temperature T , and τ_ν the dust optical depth at that frequency. The inherent assumption that $\tau \ll 1$ is reasonable at infrared wavelengths. Pixel-to-pixel variations in the measured intensity can therefore be due to varying optical depth or to varying temperature. Especially when dealing, here, with a large region containing lines of sight with large variations in temperatures, the infrared intensities are no longer useful. In order to make a first-order correction for the temperature effect, the IRAS data were analyzed with the simple approximation that large, single-temperature particles are responsible for the 60- μm and 100- μm intensities along a line of sight (Valterbos & Schwing 1987, Langer et al. 1988). Proceeding on that assumption, and further assuming that the mixture of particles is well described by the Mathis, Rumpl, and Nordsieck model (MRN 1977) and that the opacity of the dust varies as λ^{-2} , the ratio of the 60- and 100- μm intensities gives the colour temperature (T) of the dust. The optical depth τ_ν of the dust at frequency ν can then be derived from $\tau_\nu = I_\nu / B_\nu(T)$, where I_ν is the infrared intensity at frequency ν , and $B_\nu(T)$ is the Planck function intensity at that frequency ν and temperature T (see Valtorbos & Schwing 1987).

Unfortunately, the calculation of τ_ν involves assuming that the dust along the line of sight has one temperature, which is measured by the ratio of the intensities at 60 and 100 μm . This assumption obviously breaks down for lines of sight with a more complicated temperature structure.

Langer et al. (1989) examined the errors involved in this determination of dust optical depths for the case of two regions along the line of sight, each with different dust temperature. Because of the strong dependence of infrared emission on temperature, relatively small amounts of hot dust will result in more flux at the shorter wavelengths. This will influence the intensity ratio and hence the derived temperature, which will be biased towards the warm dust, even if the optical depth of the arm dust is much less than that of the cool dust. The derived value of τ is therefore an underestimate of the true dust optical depth.

A further uncertainty in the above procedure is expected from the presence of small grains of the sort proposed by Puget et al.

(1985). These grains can not only dominate the emission seen at 12 and 25 μm , but they may enhance the 60- μm emission as well (Draine & Anderson 1986). The resulting increase of the ratio of 60- and 100- μm emissivities will cause the derived optical depth to be underestimated. Because the different grain temperatures and sizes affect the optical depth in the same sense, the resulting optical depth will always be an underestimate of the true dust optical depth.

In summary, for every line of sight the intensities at 60 and 100 μm are good approximations of the dust column density, and, in regions with little temperature differences between pixels, I_{60} and I_{100} are useful to make the comparison with gas column density; in regions with a lot of pixel-to-pixel variation in the dust temperature, a better approximation of the dust column density is obtained by calculating τ_d ; because of temperature variations along each line of sight, and the presence of small dust grains, τ_d is always a lower limit to the true dust optical depth.

2.2. CO observations and visual extinction

The visual extinction was determined from Walraven photometry of a sample of 150 stars in the region of the Upper-Scorpius subgroup of the Scorpio-Centaurus OB association. The photometric observations are described in Paper I.

CO observations of the Ophiuchus molecular clouds were made using the Columbia University Sky Survey telescope on Cerro Tololo in Chile, and are reported in Paper II. The beam-size of the telescope is 8', but the observations were made at intervals of 0'.25. The area surveyed lies roughly between $l = 340^\circ$ to $+10^\circ$ and $b = 5^\circ$ to 27° . Integration times were chosen such that the rms noise temperature of the survey is 0.25 K. Figure 4 shows the resulting CO map, representing intensities integrated between -5 and 8 km s^{-1} .

2.3. H I observations of the Ophiuchus region

Information on the kinematics and distribution of the diffuse, atomic interstellar gas in the Ophiuchus region was provided by observations of the 21-cm line of H I made on the NRAO¹ 140-foot telescope during an eleven-day session in November and December, 1986. The observing technique and the data reduction and calibration procedures were similar to those described by Deul & Burton (1990). The individual H I spectra so obtained are characterized by a channel separation of 0.5 km s^{-1} , angular resolution of 20', and rms temperature values of 0.1 K. Gas column densities were derived in the standard way, assuming that the H I is optically thin.

The H I observations covered the region of interest in three separate grids. The region within $325^\circ < l < 5^\circ$ and $30^\circ < b < 40^\circ$ was sampled at intervals of 30'. The region within $324.5^\circ < l < 345.5^\circ$ and $19.5^\circ < b < 30.5^\circ$ was sampled at intervals of one degree. These two sets of data were subsequently merged with the general survey of Burton (1985) to yield data covering the entire extended region at intervals of 30'. The third observed grid covered the area of principal interest in more detail by sampling at 20' intervals within $345^\circ < l < 357^\circ$ and $15^\circ < b < 25^\circ$. Figure 5 shows the distribution of the total integrated H I column density in the same region, and on the same scale, as shown in Figs. 2 to 4.

¹ The NRAO is operated by Associated Universities, Inc., under contract with the U.S. National Science Foundation.

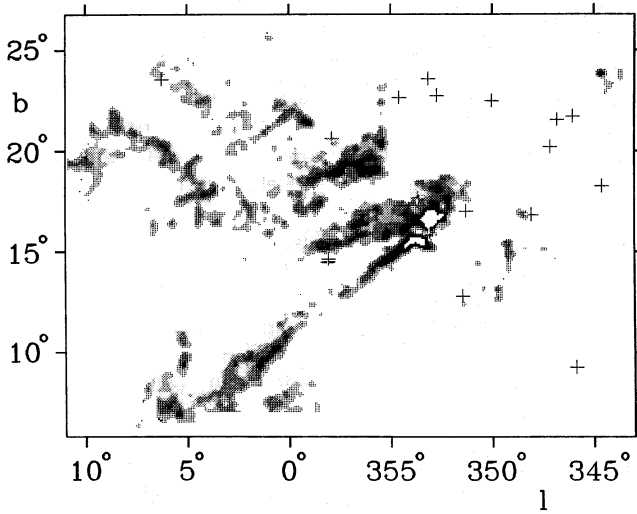


Fig. 4. Map of velocity-integrated ^{12}CO antenna temperature W_{CO} between $-8 < v < 20 \text{ km s}^{-1}$. The filamentary nature of the Ophiuchus molecular clouds is striking. The contour values are $W(\text{CO}) = 5, 20, 55,$ and $112.5 \text{ K km s}^{-1}$

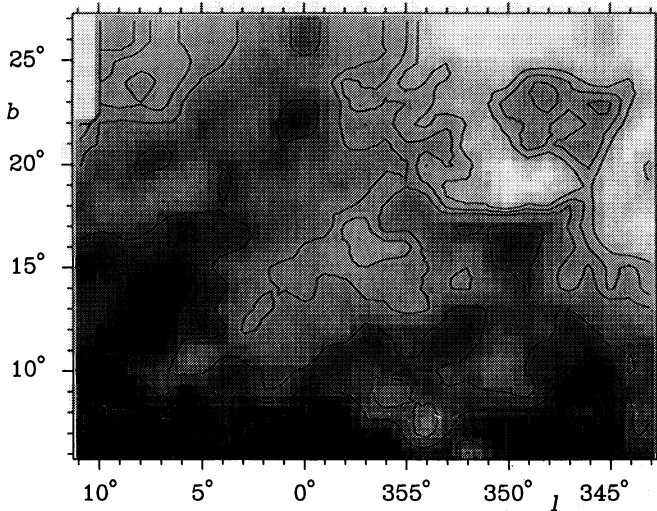


Fig. 5. Map of the distribution of the integrated H I column density in the direction of the Ophiuchus region. The atomic hydrogen distribution shows only a few similarities with the distribution of the dust. The contour values are 12.5, 13.5, 14.5, 17.5, 20, and $25 \cdot 10^{20} \text{ cm}^{-2}$

3. Correlation of the molecular and atomic gas and dust

In this section the correlation of the atomic and molecular gas and dust is investigated. First the comparison will be made on the large (Galactic) scale, followed by a comparison on the scale of the Ophiuchus region. The visual extinction and dust emission are compared in the third part of this section. The correlations of separate features in the Ophiuchus region are discussed in Sect. 4.

3.1. Global correlation

Under plausible assumptions, the dust column density is a measure of the total gas column density:

$$N_{\text{dust}} \propto (N_{\text{HI}} + 2N_{\text{H}_2}). \quad (1)$$

As was discussed in Sect. 2.1.2, the IRAS observations allow the approximations of the dust column density: the intensities at 60 and $100 \mu\text{m}$ (I_{60} and I_{100}), and the dust optical depth (τ_d). In this work, the molecular gas is traced by the integrated antenna temperature of the CO line. The conversion factor used to derive molecular hydrogen column density from the integrated CO antenna temperature

$$X = \frac{N_{\text{H}_2}}{W_{\text{CO}}} \quad (2)$$

is a much discussed number (see e.g. Bloemen et al. 1986; Sande et al. 1984; Bloemen et al. 1990; MacLaren & Wolfendale 1990). The proportionalities between the dust and the gas column densities allow us to obtain an independent determination of the conversion factor.

Along each line of sight, three interstellar components contribute to the measurements: a foreground component, a component associated with the Ophiuchus cloud, and a background component. Because the Ophiuchus region is so nearby the foreground component may be neglected. The background component is due to gas and dust associated with the general Galactic gas layer. The Galactic ensemble of molecular clouds is large and confined to an annulus whose outer boundary is effectively a kiloparsec or more from the Sun. In addition, the thickness in the z -direction of the ensemble is only some 70 pc. Consequently, at the latitude of the Ophiuchus region ($b > 6^\circ$) the CO component is not strongly influenced by the galactic background. The measured CO is therefore most likely predominantly associated with the Ophiuchus region itself. The general Galactic background does, however, have a non-negligible contribution both in the infrared and at 21-cm, which share a similar scale height, thicker than that of the molecular gas component.

3.1.1. Galactic background

Figures 6 and 7 show pixel-by-pixel comparisons of the H I column density with the $100\text{-}\mu\text{m}$ intensity and optical depth respectively for the area $l = 325^\circ$ to 20° , $b = 0^\circ$ to 35° . The high values of $N_{\text{HI}} (> 4 \cdot 10^{21} \text{ cm}^{-2})$ are all due to the lower latitudes ($b < 5^\circ$). The points at high $100 \mu\text{m}$ intensity ($> 50 \text{ MJy/sr}$) and low H I column density ($< 2 \cdot 10^{21} \text{ cm}^{-2}$) are all associated with the Ophiuchus region. Comparison with Fig. 7 makes clear that most of these high values of I_{100} at low N_{HI} are due to high dust temperature because the optical depths appear to be normal. Exclusion of these points associated with the Ophiuchus region enables the derivation of the correlation between neutral hydrogen and dust from the Galactic background in this general direction. Figures 6 and 7 show that the relations of I_{100} and τ_{100} with N_{HI} are not linear. The best fits give quadratic dependences:

$$I_{100} = 0.1 N_{\text{HI}}^2 - 0.2 N_{\text{HI}} - 1.4, \quad (3)$$

$$\tau_{100} = 9 \cdot 10^{-8} N_{\text{HI}}^2 + 3 \cdot 10^{-6} N_{\text{HI}} - 5 \cdot 10^{-5} \quad (4)$$

(with I_{100} in MJy/sr and N_{HI} in 10^{20} cm^{-2}). Linear correlation has generally been given for published values of the dust emissivity dependence on gas density. Although a linear relationship does not represent the data in Figs. 6 and 7 well, linear fits in the range of $N_{\text{HI}} \approx 10^{21}$ to $5 \cdot 10^{21}$ give $I_{100}/N_{\text{HI}} \approx 5 \cdot 10^{-1} \text{ Jy/sr/cm}^{-2}$ and $\tau_{100}/N_{\text{HI}} \approx 10^{-25} \text{ cm}^{+2}$. We note that this value of the dust-to-gas emissivity ratio, which is valid for the modes and latitudes considered here, is approximately an order of magnitude

Region	ℓ (degrees)	b	α_r	β_r	CC	X	$\alpha_{I_{100}}$	$\beta_{I_{100}}$	CC	X	$\alpha_{I_{60}}$	$\beta_{I_{60}}$	CC	X
Lower Streamer 2	all	6 - 13	3.1 ± 0.2	-6 ± 3	0.5		2.6 ± 0.1	1.8 ± 0.3	0.8	0.35	0.6 ± 0.02	0.6 ± 0.07	0.8	0.54
δ and π Sco	343 - 350	19 - 26	2.5 ± 0.3	-1 ± 3	0.5		3.3 ± 2.5	-5 ± 4	0.6		1.0 ± 0.1	-2.1 ± 0.9	0.6	
σ and τ Sco	347 - 352	13 - 19	6.3 ± 0.9	12 ± 2	0.6	0.95	4.3 ± 1.3	28.4 ± 3.5	0.5		1.1 ± 0.5	11.0 ± 1.4	0.3	
ω and β Sco	351 - 356	19 - 26	5.4 ± 1.3	3.4 ± 1.0	0.7	0.31	3.9 ± 1.1	3.3 ± 0.9	0.7	0.42	0.8 ± 0.2	0.9 ± 0.2	0.6	0.56
ν Sco	356 - 359	18 - 26	3.3 ± 1.0	3.2 ± 0.5	0.7	0.47	0.2 ± 0.7	2.9 ± 0.3	0.7		-0.3 ± 0.2	0.8 ± 0.1	0.6	
Complex 1	0 - 5	20 - 26	2.7 ± 1.1	10.8 ± 1.8	0.7		-0.4 ± 0.2	4.0 ± 0.4	0.6		-0.3 ± 0.1	0.5 ± 0.1	0.3	
Complex 5	0 - 5	15 - 20	-3.5 ± 2.1	15.3 ± 2.7	0.4		-0.5 ± 0.3	4.3 ± 0.3	0.7		-0.01 ± 0.06	0.3 ± 0.07	0.2	
ζ Oph	5 - 9	23 - 26	10.5 ± 3.4	-20.3 ± 4.1	0.8		-1.5 ± 1.0	10.4 ± 1.2	0.9		-2.3 ± 0.8	7.8 ± 0.9	0.8	
Complex 4	5 - 10	15 - 23	-2.6 ± 1.2	21.4 ± 2.1	0.7		-0.1 ± 0.2	2.4 ± 0.3	0.5		0.34 ± 0.06	-0.1 ± 0.1	0.5	
ρ Oph core	353 - 356	16 - 19	0.01 ± 5.1	11.5 ± 1.7	0.7		15.4 ± 9.4	14.6 ± 3.1	0.6		6.1 ± 3.3	4.6 ± 1.1	0.6	
Upper Streamer 2	353 - 357	12 - 16	10.6 ± 2.7	13.8 ± 1.1	0.6	0.65	12.1 ± 1.9	8.9 ± 0.8	0.6	0.37	3.1 ± 0.4	1.9 ± 0.2	0.7	0.30
Streamer 1	355 - 360	14 - 18	6.0 ± 2.0	10.6 ± 0.8	0.8	0.88	5.1 ± 1.6	5.2 ± 0.7	0.7	0.51	1.4 ± 0.5	0.9 ± 0.2	0.5	

Units: α_r : 10^{-3}cm^2 ; β_r : $10^{-3} (\text{K km s}^{-1})^{-1}$
 $\alpha_{I_{60}}$ and $\alpha_{I_{100}}$: $\text{MJy sr}^{-1} \text{cm}^2$; $\beta_{I_{60}}$ and $\beta_{I_{100}}$: $\text{MJy sr}^{-1} (\text{K km s}^{-1})^{-1}$
X : $(\text{K km s}^{-1})^{-1} \text{cm}^{-2}$

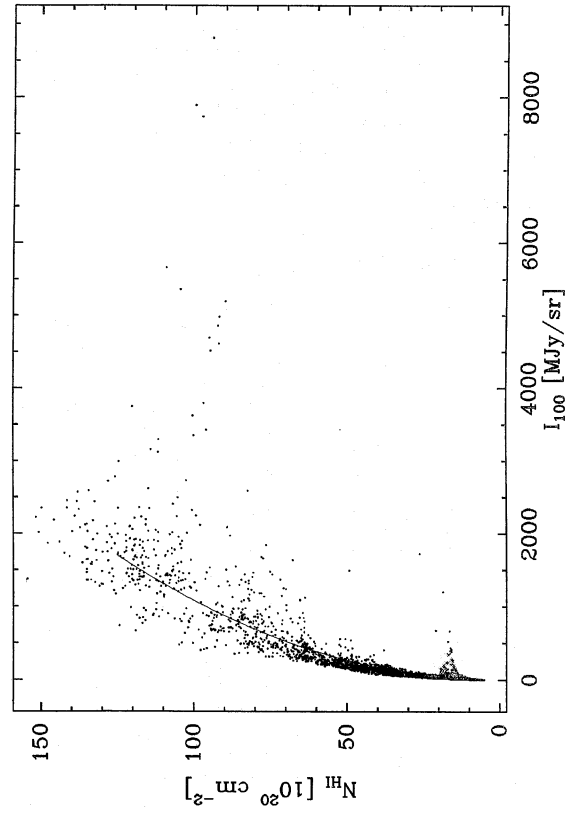


Fig. 6. Scatter plot of N_{HI} and I_{100} . The strongest intensities are caused by material close to the Galactic plane. The non-linear relation between these two parameters is mainly based on the data from the Galactic background beyond the Ophiuchus region. The relation given in Eq. (1) is based on the data in this plot

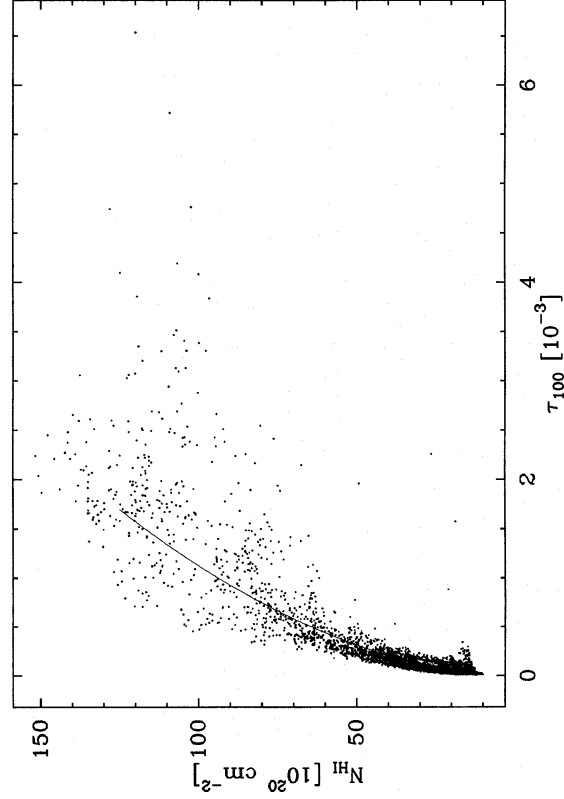


Fig. 7. Scatter plot of N_{HI} and τ_{100} . As in Fig. 6, the Galactic background dominates the correlation. The fit presented in Eq. (2) is based on this plot

higher than the values found for high-latitude interstellar cirrus structures (see e. g. Boulanger 1985; Tereby & Fich 1986; Deul & Burton 1988).

The non-linearity of the correlation and the increasing scatter at the higher values can be due to optical depth effects in the H I and variations in the interstellar radiation field. The longitude of the Ophiuchus region ($l \approx 0^\circ$) is such that the emission from long path lengths may be expected to accumulate, making optical depth effects relevant. Furthermore, the fact that the highest values in Figs. 6 and 7 are due to lower latitudes, supports this and the conclusion that variations in both the interstellar radiation field and the H I optical depth cause the increasing scatter. The Galactic background of the Ophiuchus region covers part of the inner Galaxy, so the high ratio of dust emissivity to hydrogen column density found here, compared to the ratios found in studies of the cirrus clouds, may be attributed at least in part to the higher ambient interstellar radiation flux in this direction.

3.1.2. Ophiuchus clouds

In the Ophiuchus region the presence of the molecular gas allows us to make a comparison of the dust with atomic dust molecular gas. In order to determine the dust-to-gas correlation, the expression

$$N_{\text{dust}} = \alpha N_{\text{H I}} + \beta W_{\text{CO}} \quad (5)$$

was used to approximate Eq. (1). The values of α and β were optimized simultaneously using a linear least-squares solution for the three maps. Because the dust column density can be approximated by I_{100} , I_{60} , and τ_d , we obtained three versions of Eq. (5). First, solutions were derived for the whole region. The optical depth map, Fig. 8, shows the strongest correlation. However, it is also clear that the fits are mainly determined by the regions with the highest intensities and the largest optical depths, which occur mainly in the ρ Oph core. Therefore, in order to study the correlations for the different structures separately, the maps were subdivided into separate regions. These regions will be discussed in more detail below. The results of the fits of the three dust maps with the combined gas maps, for all regions, are listed in Table 1. From Eqs. (1), (2), and (5) an expression can be derived for X :

$$X = \frac{\beta}{2\alpha} 10^{20} (\text{K km s}^{-1})^{-1} \text{cm}^{-2}. \quad (6)$$

The conversion factor X was derived for those cases where the correlation coefficient of the fit was larger than 0.6, and both the neutral hydrogen and the molecular component fit well. The values of X are listed in Table 1. In Fig. 9 the values of β and α are plotted for these cases. The line shows the best fit to the data, the dashed line corresponds to the Bloemen (1986) value of X . Based on our best fit and the spread of the data, we find a value of the conversion factor between integrated CO antenna temperature and molecular hydrogen column density, which is applicable to the Ophiuchus region: $N_{\text{H}_2} = 5^{+5}_{-2} 10^{19} W_{\text{CO}}$.

The errors in this fit introduced by the uncertainties in the subtraction of the zodiacal dust emission are small for the values based on the 100 μm intensities, but may amount to 20% and 30% for the fits to I_{60} and τ_d respectively. From Fig. 9, however, it is clear that our data points lie significantly below the line indicating the Bloemen et al. (1986) value of X , even taking these uncertainties into account. Van Dishoeck & Black (1987) showed, that the conversion factor between N_{H_2} and W_{CO} is inversely proportional to the temperature of the gas. Gas temperatures are

expected to be enhanced in this region, due to the vicinity of early-type stars in the Upper-Scorpius OB association. A low value for the factor X is, therefore, expected to be valid for the Ophiuchus clouds.

The proportionalities of the three dust components with the total gas column density are readily derived from the fits as a function of α . The average relations are:

$$\tau_d = 8 \pm 3 \cdot 10^{-26} N_{\text{H}}, \quad (7)$$

$$I_{60} = 4 \pm 3 \cdot 10^{-20} N_{\text{H}} \text{ MJy sr}^{-1}, \quad (7)$$

$$I_{100} = 6 \pm 3 \cdot 10^{-20} N_{\text{H}} \text{ MJy sr}^{-1}. \quad (7)$$

The cirrus features studied by Boulanger et al. (1985), Teret & Fich (1986), Deul & Burton (1988), and others, do show a good correlation between the dust content and the hydrogen column density. These cirrus structures are mostly heated by the general diffuse interstellar radiation field. The radiation field in the Ophiuchus clouds is much more intense than that illuminating the high-latitude cirrus, due to the proximity of the early-type stars in Upper Scorpius, and to nearby regions of active star formation. The dust temperatures are indeed higher than those which characterize typical cirrus features. The bulk of the region has a ratio of $I_{60}/I_{100} = 0.25$ which (in the MRN, λ^{-2} modified black body-spectrum model) implies a dust temperature of 24 ± 2 K. Ratios up to 0.7 are found in the Ophiuchus region, indicating temperatures as high as 40 K. The lines of sight exhibiting the high ratios are all associated with early-type stars. However, because of the large number of clouds in the region, shielding effects may also become important; such effects may cause the absence of neutral atomic hydrogen associated with the dust. We note in this regard that several separate structures are discussed in more detail below, some of which do show a correlation between their dust emissivity and total hydrogen column density, and all of which are positioned close to the early-type stars.

However, as was discussed in Sect. 2.1.2, the procedure used here to derive τ results in lower limits to the true values. This will cause the value of α to be a lower limit as well. An independent determination of the relation between the dust optical depth and the total gas column density was made by Langer et al. (1988) on the basis of a grain model by Draine & Lee (1984), and assuming that the infrared opacity is caused by graphite grains only. They derived a value $\alpha = 3.5 \cdot 10^{-25}$. Because the value of α based on our data was shown to be a lower limit to the true value, we conclude that these two determinations are consistent.

The proportionality of the dust optical depth to the total gas column density can be used to calculate the total gas particle column density associated with the dust clouds. From this the total mass of the Ophiuchus region can be derived. Using a distance of 140 pc to the Ophiuchus clouds (see Sect. 3.2), the mass derived from the dust optical depth is $2 \cdot 10^3 M_{\odot}$.

3.2. Visual extinction and emissivities

The presence of an OB association related to the Ophiuchus clouds allows us to correlate the visual extinction A_V measured towards the stars (Paper I) with the intensities measured by the IRAS satellite. Figure 10 shows A_V as a function of I_{100} . Both the visual extinction and the IRAS intensities are to some extent measures of the total amount of dust along the line of sight. Visual extinction only measures the column of dust between the observer and the star, whereas the IRAS intensities sample the entire line of sight. The difference between the measured dust columns is

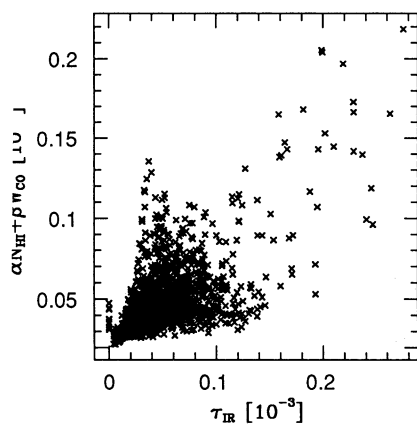


Fig. 8. Plot of the correlation between τ_d and the best fit of the H I column density and the CO intensity for the whole Ophiuchus region. The values for the best fit are: $\alpha = 2 \cdot 10^{-3} \text{ cm}^2$, and $\beta = 1.2 \cdot 10^{-2} (\text{K km s})^{-1}$

specially important in the region of the Upper-Scorpius and Ophiuchus complexes, because the stars are distributed throughout the molecular-cloud region. This will, in a lot of cases, mean that the visual extinction measures only part of the total dust column. A general relation between A_V and I_{100} or τ_{100} should be determined from the left-most data in Fig. 10 namely those with relatively low infrared emissivities. The resulting fits are:

$$\frac{I_{100}}{A_V} = 20_{-5}^{+10} \text{ MJy sr}^{-1} \text{ mag}^{-1} \quad (5)$$

$$\frac{I_{100}}{A_V} = 2.5_{-0.5}^{+2.0} \cdot 10^{-5} \text{ mag}^{-1}.$$

The ratio between I_{100} and A_V is a factor of 4 larger than the one found by Langer et al. (1988); this is probably due to the enhanced temperature of the Ophiuchus clouds, because the ratio of τ_{100} and A_V is similar to theirs. It is now possible to determine the amount of dust behind the star, as being the amount of infrared intensity measured, minus the infrared intensity expected from the measured A_V and the derived conversion factor, i. e. the shift of the points to the right of the line in Fig. 10.

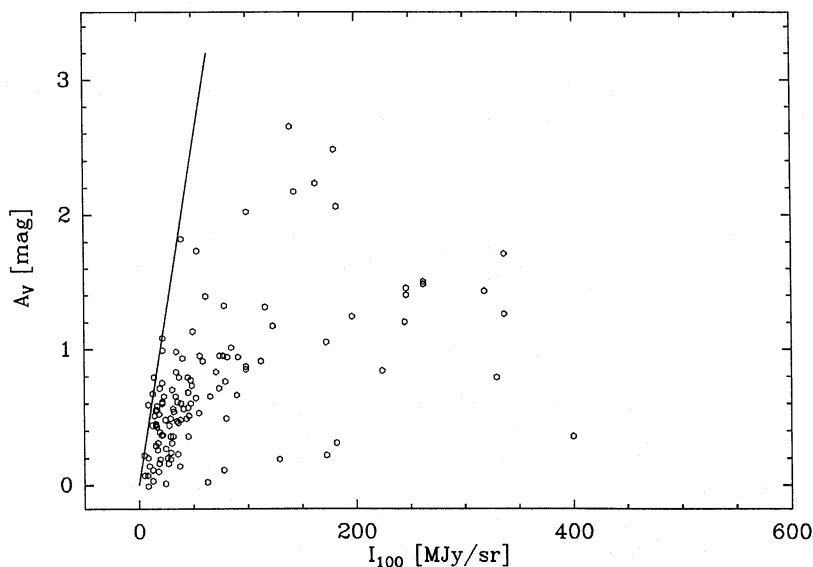


Fig. 10. Relation between the visual extinction towards the stars in Upper Scorpius and the infrared intensity at $100 \mu\text{m}$. The line is the left-best-fit to the data. The visual extinction measures only the dust column in front of the stars, whereas I_{100} measures the total dust column along those lines of sight. The dust column measured by A_V is therefore always less than or equal to that measured by I_{100}

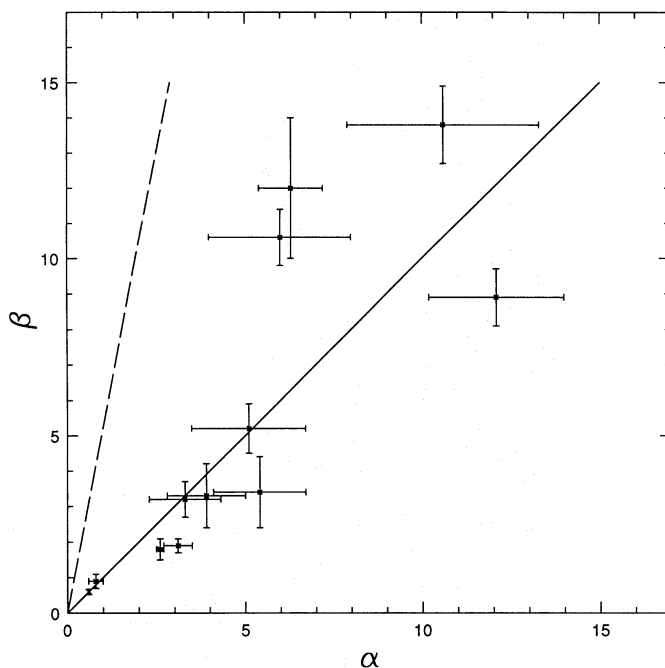


Fig. 9. Relation between the two fit parameters α and β for the fields where a good correlation was found between the dust map, the integrated CO antenna temperature and the H I column density. The best fit to the data is shown by the line, indicating the value of X reported in the text. The dashed line follows from the value of X reported by Bloemen et al. (1986). The units of α and β are given in Table 1

These considerations allow us to determine the distance to the far side of the Ophiuchus dark clouds. At the far side of the clouds, one expects the amount of excess infrared intensity to drop. The distances to the stars were derived in Paper I. Figure 11 shows the excess infrared emission for the $100\text{-}\mu\text{m}$ band. Based on the sharp drop in the amount of excess infrared intensity at a distance of 200 pc , we conclude that the molecular cloud extends up to this distance. The near edge was determined in Paper I to be 80 pc on the basis of the rise in A_V in the A_V versus distance plot. The distance of the Ophiuchus clouds is therefore 140 pc , and the full

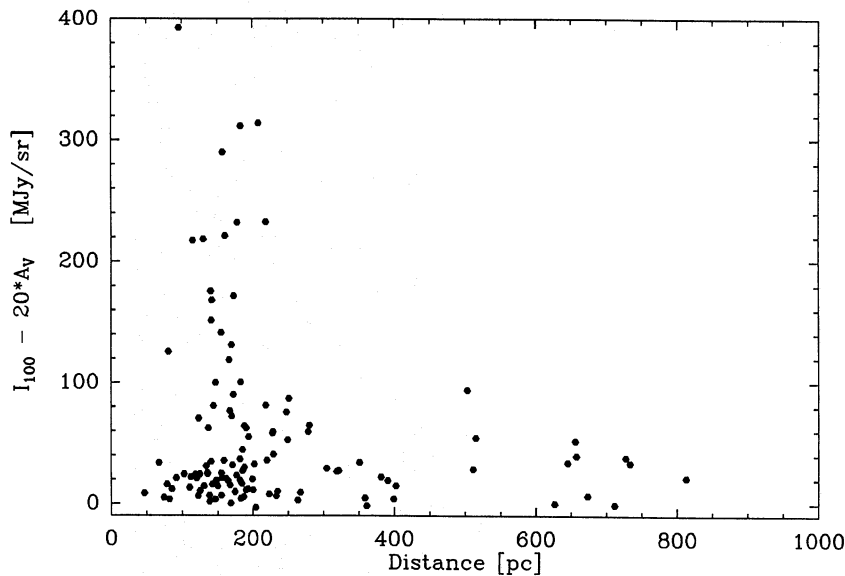


Fig. 11. Residual component of I_{100} (corrected for the component traced by A_V) plotted against the distance towards the stars. The drop in the residual component of I_{100} at approximately 200 pc implies that, at larger distances, all dust lies in front of the stars. This sets the distance of the far edge of the Ophiuchus clouds at 200 pc

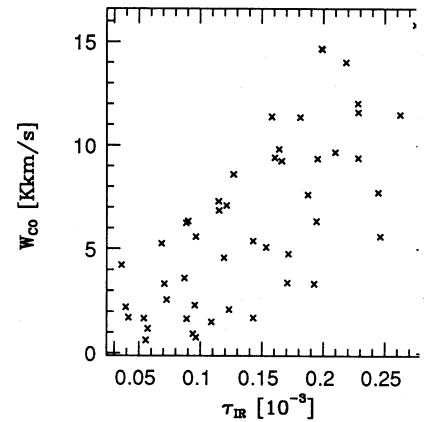


Fig. 13. Relation between the dust optical depth and the CO integrated intensity in the region of the ρ Oph core. τ_d correlates well with the molecular gas component

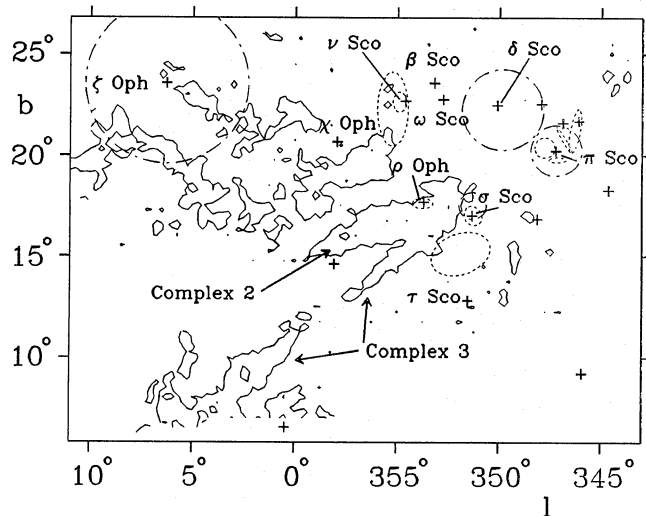


Fig. 12. Positions of the brightest stars (earlier than B2) in Upper Scorpius plotted (pluses), together with the lowest contour of $W(\text{CO})$ (thick line). The dash-dotted lines outline the H II regions in Sharpless's catalogue (1959); the dotted lines show the bright nebulae from Lands's catalogue (1965)

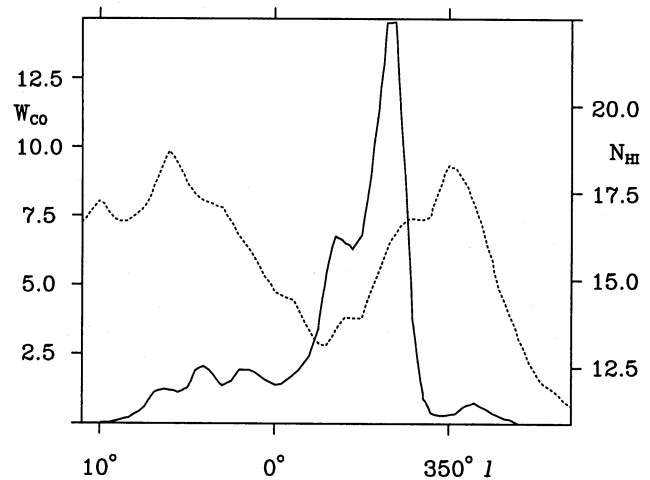


Fig. 14. Distribution of W_{CO} (full line, units in K km s^{-1}) and N_{HI} (dotted line units in 10^{20} cm^{-2}) as a function of l at constant $b = 16.5^\circ$. Note the offset in the peaks of the atomic and molecular gas components

depth is approximately 120 pc. The Ophiuchus/Upper-Scorpius complex spans an angle of 30° on the sky, which corresponds to a tangential size of approximately 80 pc. Within the errors, the tangential and radial sizes are similar.

4. Comparison of individual structures in the Ophiuchus region

In this section, separate structures in the Ophiuchus region will be discussed. The nomenclature is based, in part, on identification of clouds and complexes in Paper II. Figure 12 shows the positions and names of the most important structures and stars in the

region. The results of the correlations between the two gas components and the dust, for each of the separate structures, are listed in Table 1.

4.1. ρ Ophiuchus cloud

The densest part of the Ophiuchus clouds lies in the heart of the Ophiuchus/Upper-Scorpius region near $(l, b) = (353^\circ, 17^\circ)$, and is known as the ρ Oph cloud. Several early-type stars are located near or inside the cloud, such as the highly extinguished star HD 147889, and ρ Oph itself. Several studies have revealed the presence of pre-main sequence objects inside the cloud (e.g.

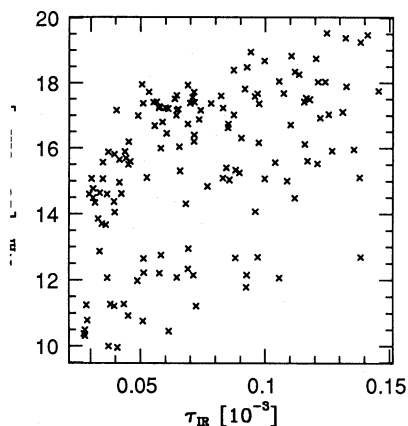


Fig. 15. Plot of the dust optical depth as a function of the H I column density in the direction of the stars σ and τ Sco. The two components are weakly correlated

rasdalen et al. 1973; Vrba et al. 1975; Elias 1978; Wilking & Lada 1983). As expected from the proximity of the early-type stars and ongoing star formation, the ratio of 60 to 100 μm is relatively high. With the assumptions listed in Sect. 2.1.2, dust temperatures are found as high as 30 K.

The comparison of the different tracers shows a strong correlation between the dust optical depth and the total gas column density, which is mostly due to a strong correlation between the CO and the dust (Fig. 13), N_{HI} appears to be uncorrelated with the dust in this region. Due to the strong pixel-to-pixel variation of the dust temperature in this region, the IRAS intensities have a much weaker correlation with the total gas column density.

2. Complexes 2 and 3

Complexes 2 and 3, identified in Paper II, are the elongated structures pointing away from the region of early-type stars. Vrba et al. (1976), and Vrba (1977) considered the origin of these elongated structures to be most likely caused by the passage of a shock (see also de Geus 1991). Comparison of the spatial distribution of the dust and the two gas components shows that the elongated molecular clouds are offset from a similarly elongated feature in the neutral hydrogen. The features in the IRAS 100- μm map are well correlated with the total gas column density. A cut at constant b through the structures (i.e. almost perpendicular to their elongation) shows the offset between H I and CO very clearly (Fig. 14). The structures have no known embedded heat sources; their heating is likely provided by the stars in Upper Scorpius.

The gas mass derived from the total dust optical depth is $30 M_{\odot}$.

3. Region around σ and τ Sco

The early-type stars σ Sco, with spectral type B1 III, and τ Sco, spectral type B0 V, are located adjacent to the ρ Oph cloud. The stars are surrounded by the H II regions S9 and RCW 129, respectively, which are clearly visible on the H α -photographs of Ivan (1974, see Fig. 13 of Paper II). The IRAS maps reveal a significant amount of flux in this region. Very little CO was found, however, and all of it is located in small clouds at the edge of the region of strong dust emission. The ratio of the 60- and 100- μm intensities indicates a dust temperature of 38 K near σ Sco. Not

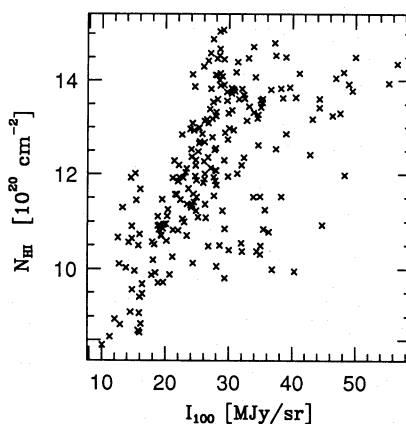


Fig. 16. Infrared intensity at 100 μm as a function of H I column density for the region around the stars π and δ Sco. The two components are weakly correlated

surprisingly, therefore, the IRAS intensities show no correlation with the total gas column density. The dust optical depth, on the other hand, does. Because of the sparseness of the CO, this correlation is mostly due to the atomic component (Fig. 15).

The structure of this region suggests the destruction of a molecular cloud by young stars. Centered upon the two bright stars are two H II regions, surrounded by a cloud of atomic hydrogen with the molecular component restricted to small clumps at the edge of the structure. Interestingly, the entire complex of ionized, atomic, and molecular gas is pervaded by dust, which is evident from the infrared maps.

4.4. Region around π and δ Sco

The area around the stars π Sco, with spectral type B1 V, and δ Sco, of spectral type B0.3 IV, is in many ways similar to the region around σ and τ Sco. The IRAS maps show a considerable amount of emission, but very little CO was observed associated with it. One small cloud was found located at the edge of the region, at $(l, b) = (344^{\circ}, 24^{\circ})$; this is the CO cloud with the widest lines (FWHM = 4.5 km s^{-1}) found in the entire region. Both π and δ Sco are surrounded by H II regions (S1 and S7, respectively). The 60- to 100- μm intensity ratio suggests that most of the dust has temperatures $> 25 \text{ K}$. The infrared intensities are well correlated with an H I cloud, as can be seen from Fig. 16, the plot of I_{100} versus N_{HI} . The correlation of the dust optical depth with the gas column density is weak, which might be due to the presence of small dust particles.

The uncharacteristically wide lines of the CO cloud associated with the region suggest that it is in the process of being destroyed. Furthermore, the appearance of the region, with the H II regions around the two early-type stars, all surrounded by an H I cloud, with a small, clearly unstable molecular cloud at its edge, and the region generally pervaded by dust, does give the impression of being the remnant of a molecular structure, being destroyed by the massive stars embedded in it.

4.5. Region around ν Sco

The early-type star ν Sco lies at the low-longitude edge of the reflection nebula IC 4592, which is spatially correlated with a dust cloud. At the high-longitude edge of this cloud, furthest away from the early-type stars, two small CO clouds were observed. All

three tracers of the dust column density correlate with the gas column density (see Table 1).

4.6. Region around ζ Oph

ζ Oph is a runaway star of the Upper-Scorpius subgroup of the Scorpio-Centaurus OB association (Blaauw 1961); it is the only O star (spectral type O9.5V) of the association. At the position of the star the CO map shows a gap in an otherwise elongated structure (complex 1E, see Paper II). This gap correlates with a small H I cloud with a velocity of 3 km s^{-1} . A particularly strong feature in both the 60- and 100- μm maps covers part of the elongated CO structure, and the gap. The ratio of the two infrared intensities is large, indicating a dust temperature of 34 K. Again the picture of photodissociation of part of the elongated molecular cloud by the bright star appears likely.

The pixel-by-pixel comparison of the CO and the dust tracers in this region shows a very interesting property. The CO appears to correlate well with both the 60- and 100- μm intensities, but shows an *anti*-correlation with the dust optical depth map. The temperature effect on the dust emissivity would have given the opposite result, the optical depth would have then correlated better with the gas, as seen for instance in the region around σ and τ Sco. One possible explanation for the anti-correlation between the CO and the dust optical depth could be an under-estimate of the temperature of the dust, as determined from the 60- to 100- μm intensity ratio. This could be caused by the presence of a component of cold dust along the line-of-sight, not associated with any CO detectable in the mm-wavelength range, but with a component strong enough at 100- μm to cause a decrease of the 60- to 100- μm ratio. An alternative explanation might be that in this particular cloud the dissociation of the CO has proceeded further than the destruction of the dust grains, resulting in an apparent lack of molecules with respect to dust grains.

5. Conclusions

Interstellar gas and dust in the direction of the Ophiuchus region was investigated using IRAS skyflux maps, 21-cm data, and observations of ^{12}CO . The H I and the infrared emission from the Galactic background to the Ophiuchus region generally show a correlation, which can be fit by a second-order polynomial. The ratios of both the intensity and dust optical depth at 100 μm to the neutral hydrogen column density are a factor ten larger than values published for cirrus features. This difference can be attributed to properties of the dust particles in a heated environment. From the assumption that the dust optical depth is proportional to the total gas column density, the conversion factor between W_{CO} and N_{H_2} was derived. The conversion factor was found to be a factor of five smaller than the one found by Bloemen et al. (1986). Because the conversion factor is inversely proportional to temperature (van Dishoeck & Black 1987), the Bloemen et al. (1986) value can be considered to be an upper limit in the hot environment of the Ophiuchus clouds. From a comparison of the visual extinction towards the stars with the infrared intensities in the same directions, the distance of the far edge of the Ophiuchus complex was determined to be 200 pc.

Several individual regions were discussed, each with different properties of the gas-to-dust correlations. The two elongated structures characterizing the Ophiuchus clouds were shown to be spatially correlated with a gap in the H I distribution. The gap in the H I lies on the side of the dense ϱ Oph cloud opposite to the

stars. Three regions, that are positioned close to the early-type stars of the Upper-Scorpius subgroup, were discussed. The regions are characterized by an underabundance of CO compared to the dust optical depth. The dust clouds found in these regions are hot, and are all spatially correlated with clouds of neutral hydrogen. A plausible explanation for this is that the H I clouds are the photodissociated remnants of a molecular cloud, of which the ^{12}CO is fully dissociated, and the dust is heated but not destroyed. Relatively far away from the early-type stars another region is characterized by the presence of elongated structure associated both with ^{12}CO and H I clouds. The clouds are probably associated with the high-longitude edge of an H I loop around the Upper-Scorpius stars. The presence of this H I loop is discussed further by the Geus (1991). We suspect that the early-type star ζ Oph has dissociated part of one of the elongated structures, leaving a hot dust cloud associated with a cloud of neutral hydrogen.

Acknowledgements. We are grateful to Drs. A. Blaauw, P.T. de Zeeuw, and E.F. van Dishoeck for comments on a draft version of this paper. EdG acknowledges partial financial support by NS grant AST 8618763 and NSA grant JPL 958009.

References

- Baart E.E., de Jager G., Mountfort P.I., 1980, A & A 92, 156
 Blaauw A., 1961, Bull Astron. Inst. Neth. 15, 265
 Blaauw A., 1964, ARA & A 2, 213
 Bloemen J.B.G.M., Strong A.W., Cohen R.S., Dame T.M., Grabelsky D.A., Hermsen W., Lebrun F., Mayer-Hassewander H.A., Thaddeus P., 1986, A & A 154, 25
 Bloemen J.B.G.M., Deul E.R., Thaddeus P., 1990, A & A (in press)
 Boulanger F., Baud B., van Albada G.D., 1985, A & A 144, 9
 Boulanger B., Perault M., 1988, ApJ (in press)
 Burton W.B., 1985, A & AS 62, 365
 Burton W.B., Deul E.R., 1987, in: The Galaxy, eds. G. Gilmore, B. Carswell, Reidel, Dordrecht, p. 141
 Burton W.B., Liszt H.S., 1983, A & AS 52, 63
 Cappa de Nicolau C.E., Pöppel W.G.L., 1986, A & A 164, 27 (CdNP)
 Colomb F.R., Pöppel W.G.L., Heiles C., 1980, A & AS 40, 47
 de Geus E.J., de Zeeuw P.T., Lub J., 1989, A & A 216, 44 (Paper I)
 de Geus E.J., Bronfman L., Thaddeus P., 1990, A & A 231, 13 (Paper II)
 de Geus E.J., 1991, A & A (submitted) (Paper IV)
 Deul E.R., Burton W.B., 1988, in: E.R. Deul's Ph.D. Thesis: University of Leiden, Chap. 7
 Deul E.R., Burton W.B., 1990, A & A 230, 153
 Deul E.R., Wolstencroft R.D., 1988, A & A 196, 277
 Draine B.T., Anderson N., 1985, ApJ 292, 494
 Draine B.T., Lee H.M., 1984, ApJ 285, 89
 Elias J.H., 1978, ApJ 224, 453
 Grasdalen G.L., Strom K.M., Strom S.E., 1973, ApJ 184, L5
 Hauser M.G., Silverberg R.F., Stier M.T., Kelsall T., Gezari D.Y., Dwek E., Walser D., Mather J.C., 1984, ApJ 285, 74
 Hildebrand R.H., 1983, Quart. J.R. Astron. Soc. 24, 267
 IRAS Explanatory Supplement, 1984, eds. C. Beichman, G. Neugebauer, H.J. Habing, P.E. Clegg, T.J. Chester, JPL D 1855
 Langer W.D., Wilson R.W., Goldsmith P.F., Beichman C.A., 1989, ApJ 337, 355

- Lynds B.T., 1965, ApJS 12, 163
MacLaren I., Wolfendale A.W., 1990, A & A (in press)
Maganian L., Blitz L., Mundy L., 1985, ApJ 295, 402
Mathis J.S., Rimpl W., Nordsieck K.H., 1977, A & A 217, 425 (MRN)
Mouget J.L., Leger A., Boulanger F., 1985, A & A 142, L19
Nodders A.W., Campbell C.T., Whiteoak J.B., 1960, MNRAS 121, 103
Osterman D.B., Solomon P.M., Scoville N.Z., 1984, ApJ 276, 182
Pavani B.D., Mathis J.S., 1979, ARA & A 17, 73
Phillips S., 1959, ApJS 4, 257
Rivard J.P., 1974, ApJS 16, 163
Rodriguez T.J., Dwek E., Hauser M.C., Kerr F.J., 1988, ApJ (in press)
Terebey S., Fich M., 1986, ApJ 309, L73
van Dishoeck E.F., Black J.H., 1987, in: Physical Processes in Interstellar Clouds, NATO ASI series vol. 210, eds. G.E. Morfill, M. Scholer, p. 241
Vrba F.J., 1977, AJ 82 (3), 198
Vrba F.J., Strom K.M., Strom S.E., Grasdalen G.L., 1975, ApJ 197, 77
Vrba F.J., Strom S.E., Strom K.M., 1976, AJ 81 (11), 958
Walterbos R.A.M., Schwing P.B.W., 1987, A & A 180, 27
Williams D.R.W., 1973, ApJS 8, 505
Wilking B.A., Lada C.J., 1983, ApJ 274, 698